Available online at www.sciencedirect.com

ScienceDirect

Transportation Research Procedia 70 (2023) 406–413

Transportation Research Procedia

www.elsevier.com/locate/procedia

8th International Electric Vehicle Conference (EVC 2023)

Analysing unbalanced ageing in EV battery Packs using the Low-Cost Lumped Single Particle Model (LSPM): the impact of temperature gradients among parallel-connected cells

Haosong He[a,*], Xiangjie Chen[a]

[a]*Centre for Renewable Energy Systems Technology (CREST), Wolfson School, Loughborough University, Loughborough, LE11 3GR*

Abstract

Lithium-ion battery cells are widely used in electric vehicles (EVs) due to their high energy density and long lifespan. However, these cells are sensitive to temperature and can age at different rates depending on the temperature they are subjected to. While EV battery packs are equipped with a battery thermal management system (BTMS) to regulate the temperature of the pack, it cannot completely eliminate temperature gradient within the pack due to the limited cooling capabilities. As a result, a maximum temperature gradient of 5 °C is allowed in BTMS designs for EVs, which leads to uneven ageing speeds within the pack. Due to practical limitations of battery management system (BMS), it is difficult to directly measure the currents flowing through each parallel-connected cell, making it challenging to actively balance the cells. To investigate the pack-level current distribution and ageing trends caused by temperature gradient, this paper adopts the low computational cost Lumped Single Particle Model (LSPM) coupled with Arrhenius dependency to investigate the influence of temperature on current distribution as well as the resulting unbalanced ageing rates among parallel-connected cells in a 4s6p Panasonic NCR18650PF battery pack.

Keywords: Lithium-ion battery pack; Ageing; Parallel-connected cells

1. Introduction

Lithium-ion cells offer numerous advantages, including high energy density (100-265 Wh/kg) Zhou et al. (2022), long cycle life (> 1,000 cycles) Tang et al. (2022), and low self-discharge rate Shan et al. (2022), which have made them as the preferred power source for electric vehicles (EVs). Nevertheless, cell ageing remains a significant concern in the EV industry due to the decline in performance over time, resulting from irreversible physical and chemical changes. To mitigate ageing, cells are connected in parallel and series within an EV battery pack, significantly reducing the discharging C-rate while maintaining the required power output. For instance, a Tesla Model S battery pack

*Xiangjie Chen. Tel.: +441509227558.
E-mail address: X.J.Chen@lboro.ac.uk

2352-1465
10.1016/j.trpro.2023.11.046

comprises 16 modules, each containing 74 parallel-connected 18650 cell units and six series-connected units (74p6s) He et al. (2023). However, employing numerous cells also introduces cell inconsistency issues.

Although fresh cells from the same batch typically exhibit similar electrochemical properties, such as effective capacity and internal resistance, unavoidable internal differences may arise from variations in production processes or operating conditions, including temperature gradients and current loads Jafari et al. (2018). For example, among 20,000 fresh cells, the measured initial capacity demonstrated a normal distribution with a 1.3% deviation, while the direct current internal resistance exhibited the same distribution with a 5.8% deviation Jafari et al. (2018). Temperature gradients and current loads can lead to variations in electrochemical properties among cells, such as internal ohmic resistance, charge exchange current, and diffusion time constant, thereby causing current maldistribution Ekström et al. (2018). Intrinsic factors, such as production process-related internal differences, and extrinsic factors, including temperature gradients and current maldistribution, can be actively mitigated by a battery thermal management system (BTMS) and a battery balancing system (BBS), respectively Ziegler et al. (2021). BBS can reduce cell-to-cell variations during battery operation, resulting in up to 3.1% higher effective capacity and 7.7% longer service life Ziegler et al. (2021).

In controlling current maldistribution, BBS typically measures and balances voltages for series-connected units but cannot measure currents among parallel-connected cells due to the impracticality and cost of adding extra current sensors Gong et al. (2014); Yang et al. (2016). Consequently, current maldistribution among parallel-connected cells accelerates uneven ageing, pack-level degradation, and ultimately, the EV's lifespan reduction. For example, a 20% difference in the state of health (SOH) between two parallel-connected cells could lead to cells operating at 40% higher current, increasing heat and reducing battery pack reliability Gong et al. (2014). Ekström et al. Ekström and Lindbergh (2015) found that a cell aged four times faster at 45 °C compared to 25 °C.

Most studies, however, focus on configurations with parallel connections only, failing to accurately represent real-world applications wherein current maldistribution can be more complex due to combined serial and parallel connections Zhu et al. (2023). In this study, we adopted a model consisting of 4p6s 18650 cells cooled by a liquid BTMS with a serpentine-shaped cooling pipe. This paper numerically investigates the influence of temperature gradients on current distribution and uneven ageing speed among cells at the pack level, revealing that temperature gradient contributes to uneven ageing rate.

2. Model Development

The specification of the battery pack is given in Table 1. Fig. 1 illustrates the battery pack (4p6s) configuration where the cells are wrapped by an aluminium cooling pipe, cells are connected to the steel busbar connectors on the top and bottom surfaces throughout the steel terminals. The simulations of this work are finished on COMSOL Multiphysics 6.1.

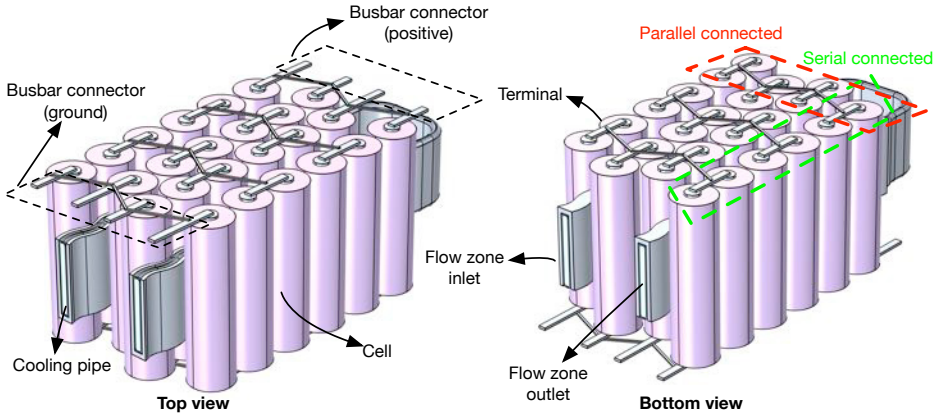

Fig. 1. Schematic views of the coupled model: cells are configured in 4s6p, where the top and bottom surfaces are connected to the steel busbar throughout the steel terminals, and wrapped by an aluminium cooling pipe.

Table 1. Battery pack specification.

Property	Value	Single cell State of Charge - Open Circuit Voltage (SOC-OCV)
Configuration	4p6s	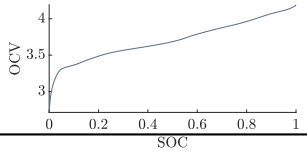
Capacity	11.96 Ah	
Min/max voltage	15 V / 25.2 V	
Cathode material	NCA	
Anode material	Graphite	

The values of properties, specifications parameters of the battery pack used in simulations are presented in Table 2.

Table 2. Values of properties, specifications parameters of the battery pack used in simulations

Property	Symbol and unit	Value	Source
Cell			
Ohmic overpotential at 1C	$\eta_{ohm,1C}$ (mV)	51.7	Fitted
Charge exchange current rate	J_0(-)	0.3	Fitted
Diffusion time constant	τ (s)	6712	Fitted
Activation energy	$E_{act}^{\eta_{ohm,1C}}$ $(kJmol^{-1})$	24.36	Fitted
Activation energy	$E_{act}^{J_0}$ $(kJmol^{-1})$	-58.98	Fitted
Activation energy	E_{act}^{τ} $(kJmol^{-1})$	18.58	Fitted
Calendar ageing time constant	τ_{loss} (s)	1.5812×10^8	Gümüşsu et al. (2017)
Offset potential	E_{offset} (V)	0.36119	Fitted
Transfer coefficient	α $(-)$	0.31005	Fitted
Capacity fade rate	G $(-)$	49.679	Fitted
Additional capacity loss	H $(-)$	0.0021459	Fitted
Activation energy	E_a $(kJmol^{-1})$	56.227 (25 °C - 45 °C)	Fitted
Density	ρ_{batt} (kgm^{-3})	2939	Gümüşsu et al. (2017)
Heat capacity	$C_{p,batt}$ $(Jkg^{-1}K^{-1})$	1400	Fitted
Radial thermal conductivity	k_r $(Wm^{-1}K^{-1})$	1	Al-Zareer (2020)
Axial thermal conductivity	k_a $(Wm^{-1}K^{-1})$	30	Al-Zareer (2020)
Module			
Initial state of charge	SOC_0	1	-
Cell initial capacity	$Q_{cell,0}$ (Ah)	11.96	-
Reference temperature	T_{ref} (°C)	25	-
Initial temperature	T_0 (°C)	25	-
Coolant			
Density	ρ_{cool} (kg m^{-3})	1.184	-
Heat capacity	$C_{p,cool}$ $(Jkg^{-1}K^{-1})$	2400	-
Thermal conductivity	k_{cool} $(Wm^{-1}K^{-1}$	0.026	-
Dynamic viscosity	μ_{cool} $(Jkg^{-1}K^{-1})$	1.002	-
Inlet velocity	$\vec{v}_i$ (ms^{-1})	0.01	-
Connector & terminal			
Density	ρ_{con} (kg m^{-3})	7850	-
Heat capacity	$C_{con,air}$ $(Jkg^{-1}K^{-1})$	475	-
Thermal conductivity	k_{con} $(Wm^{-1}K^{-1})$	44.5	-
Cooling pipe			
Density	ρ_{pipe}, ρ_{bus} (kg m^{-3})	2700	-
Heat capacity	$C_{p,pipe}, C_{p,bus}$ $(Jkg^{-1}K^{-1})$	900	-
Thermal conductivity	k_{pipe}, k_{bus} $(Wm^{-1}K^{-1})$	238	-

The total overpotential is pertinent to ohmic, activation and concentration overpotential, which relates to the irreversible heat in cell and given by:

$$\eta = \eta_{ohm} + \eta_{act} + \eta_{conc} \tag{1}$$

Here, the ohmic overpotential (η_{ohm}) is due to resistances (R_{ohm}) in the movement of ions and electrons, as described by Ohm's law, given by:

$$\eta_{ohm} = R_{ohm} I_{batt} = \frac{\eta_{ohm,1C}}{I_{1C}} I_{batt} \tag{2}$$

, where I_{batt} is the applied current, I_{1C} is 1C current, $\eta_{ohm,1C}$ is the ohmic overpotential for 1C current of the cell.

The activation overpotential (η_{act}) reflects the activation barrier in the electrochemical reactions taking place in the cell, given by:

$$\eta_{act} = \frac{2RT}{F} arcsinh(\frac{I_{batt}}{2J_0 I_{1C}}) \tag{3}$$

, where R is the molar ideal gas constant, F is the Faraday constant, T is the absolute temperature of cell, J_0 is the dimensionless charge exchange current rate.

The concentration overpotential (η_{conc}) is caused by the finite transport rates of reacting material within the cell, and can be calculated by applying Fick's diffusion equation to a dimensionless local particle SOC (S) over a one-dimensional particle length of 1. The equation incorporates a dimensionless spatial variable X, which varies from 1 (particle surface) to 0 (particle center), given by:

$$\tau \frac{dS}{dt} = \nabla^2 S \tag{4}$$

, where τ is the diffusion time constant. The boundary conditions are given by:

$$\nabla S|_{X=0} = 0 \tag{5}$$

$$\nabla S|_{X=1} = -\frac{\tau I_{batt}}{N_{shape} Q_{batt,0}} \tag{6}$$

, where N_{shape} is 3 for the spherical coordinate in this study, $Q_{batt,0}$ is the cell capacity.

The battery average SOC (SOC_{ave}) is obtained by integrating over the volume of the particle, is given as:

$$SOC_{ave} = 3 \int_0^1 S^2 dX \tag{7}$$

Therefore, the concentration overpotential (η_{conc}) is given by:

$$\eta_{conc} = E_{OCV}(S|_{X=1}, T) - E_{OCV}(SOC_{ave}, T) \tag{8}$$

The entropy change of the cell is given by:

$$E_{entropy} = (T - T_{ref}) \frac{\partial E_{OCV}(SOC_{ave})}{\partial T} \tag{9}$$

, where the entropy coefficient of the Panasonic NCR18650PF cell is taken from Ref. Lu et al. (2019), and listed in Table 3.

Table 3. Variation of the entropy coefficient with SOC Gümüşsu et al. (2017).

SOC_{ave}	1	0.9	0.8	0.7	0.6	0.5	0.4	0.3	0.2	0.1	0
$\frac{\partial E_{OCV}(SOC_{ave})}{\partial T}$ (mVK^{-1})	-1.62	0	0	0	0	1.02	1.02	1.38	0	0	0

Thus, the open circuit voltage (OCV) under various temperatures is the sum of reference OCV and the entropy voltage change, given by:

$$E_{OCV}(SOC_{ave}, T) = E_{OCV,ref}(SOC_{ave}) + E_{entropy} \tag{10}$$

The terminal voltage (E_{batt}) can be calculated by the sum of the overpotential and the OCV, given by

$$E_{batt} = E_{OCV,ref}(SOC_{ave}) + E_{entropy} + \eta_{ohm} + \eta_{act} + \eta_{conc} \tag{11}$$

The electrochemical parameters ($\eta_{ohm,1C}$, J_0 and τ) applied in LSPM are temperature sensitive, which can be modelled by coupling the Arrhenius dependency Ekström et al. (2018). Arrhenius dependency relates the temperature sensitive parameters of the cell at present temperature to that parameters at a reference temperature via an exponential function with activation energy E_{act} Ekström et al. (2018), given by:

$$\eta_{ohm,1C} = \eta_{ohm,1C,ref}\ exp[\frac{E_{act}^{\eta_{ohm,1C}}}{R}(\frac{1}{T} - \frac{1}{T_{ref}})] \tag{12}$$

$$J_0 = J_{0,ref}\ exp[\frac{E_{act}^{J_0}}{R}(\frac{1}{T} - \frac{1}{T_{ref}})] \tag{13}$$

$$\tau = \tau_{ref}\ exp[\frac{E_{act}^{\tau}}{R}(\frac{1}{T} - \frac{1}{T_{ref}})] \tag{14}$$

, where $\eta_{ohm,1C,ref}$, $J_{0,ref}$ and τ_{ref} represent their values under the reference temperature.

The solid electrolyte interphase (SEI) formation on cell anode is the primary cause of battery degradation, which mainly depending on cell voltage, current, and temperature Ekström and Lindbergh (2015). The ageing model proposed by Ekström et al. Ekström and Lindbergh (2015) considers the capacity loss (Q_{loss}) associated with the parasitic SEI formation. Q_{loss} can be described by a integration of the parasitic SEI current (I_{loss}) over the time, given by:

$$Q_{loss} = \int I_{loss}\partial t \tag{15}$$

Here, I_{loss} is given by:

$$I_{loss} = \frac{\partial Q_{cell,0}}{\tau_{loss}} f \tag{16}$$

, where τ_{loss} is a calendar ageing time constant defining the rate of the parasitic reactions, and f is the ageing factor. Typically, capacity loss associates with the cell voltage, the capacity throughput, ageing history and temperature, described by the dimensionless ageing factors: f_E, f_I, f_{aged}, f_T, respectively COMSOL (2022), given by:

$$f = f_E f_I f_{aged} f_T \tag{17}$$

Here, f_E represents the result of either a parasitic electrochemical reduction reaction occurring on the negative electrode, or an oxidation reaction occurring on the positive electrode, given by:

$$f_E = exp(\frac{\alpha F(E_{OCV}(SOC,T) + \eta_{act} - \overline{E_{OCV}}(T) - E_{offset})}{RT}) \tag{18}$$

Here, the transfer coefficient (α) and offset potential (E_{offset}) parameters relate how the rate of the parasitic reactions changes when the battery voltage deviates from the average open circuit voltage ($\overline{E_{OCV}}(T)$), given by:

$$\overline{E_{OCV}}(T) = \int_0^1 E_{OCV}(SOC,T)\partial SOC \tag{19}$$

f_I represents the linear relation between the capacity fade and the number of full cycles, given by:

$$f_I = 1 + H\frac{\tau_{loss}|I_{batt}|}{2Q_{cell,0}} \tag{20}$$

, where H is the additional (dimensionless) capacity loss induced by cycling.

f_{aged} represents the rate of the capacity fade slowed down by the parasitic reactions, e.g. the formation of a mass transport limiting film on the electrode particles, given by:

$$f_{aged} = \frac{1}{1 + (G-1)\frac{Q_{loss}}{Q_{cell,0}}} \tag{21}$$

, where G is how many times the capacity fade rate has been reduced when all capacity has been lost.

f_T is the ageing caused by temperature describing by an Arrhenius expression, given by:

$$f_T = exp(-\frac{E_{act}}{R}(\frac{1}{T} - \frac{1}{T_{ref}})) \tag{22}$$

, where E_{act} is the activation energy.

According to Bernardi's heat generation modelBernardi et al. (1985) total heat generation (Q_{total}) from cell consists of the irreversible heat (Q_{irrev}) and the reversible heat (Q_{rev}). Q_{irrev} is caused by COMSOL (2022): 1) Ohmic losses in the electrolyte, electrodes, and current collectors ($Q_{\eta_{ohm}}$), 2) activation losses for the charge transfer reactions ($Q_{\eta_{act}}$), and 3) local gradients in composition generating heat due to non-ideal effects of mixing (Q_{mix}) , given by:

$$Q_{irrev} = Q_{\eta_{ohm}} + Q_{\eta_{act}} + Q_{mix} \tag{23}$$

, where:

$$Q_{\eta_{ohm}} = \eta_{ohm} I \tag{24}$$

$$Q_{\eta_{act}} = \eta_{act} I \tag{25}$$

$$Q_{mix} = \frac{N_{shape} Q_{cell,0}}{\tau_{Arrh}} \int_0^1 \frac{\partial E_{OCV,therm}}{\partial S} \frac{\partial S}{\partial X} \frac{\partial S}{\partial X} X^{N_{shape}-1} \partial X \tag{26}$$

Here, the thermo neutral voltage is given by:

$$E_{OCV,therm} = E_{OCV,ref}(S) - T_{ref} \frac{\partial E_{OCV}(S)}{\partial T} \tag{27}$$

Q_{rev} is caused by the entropy changes in the electrode reactions, given by:

$$Q_{rev} = T \frac{\partial E_{OCV}(S|_{x=1})}{\partial T} I \tag{28}$$

3. Result and discussion

In this section, the uneven ageing of a battery pack caused by a temperature gradient is investigated. A water-cooling system with an inlet temperature of 25°C and a flow rate of 0.01 ms^{-1} is employed to cool the pack. For the ensuing analysis, the representative cells are chosen as $Cell_{1,1}$, $Cell_{4,1}$, and $Cell_{1,6}$, as shown in Fig. 2a. The pack undergoes a cycling protocol comprising a 0.5C constant current (CC) charge, a 4.2V constant voltage (CV) charge with a 0.05C cutoff, a 1C discharge to 2.5V, and a 30-minute rest period over 30 days. Fig. 2b delineates the full cycle of voltage, current, and temperature variation.

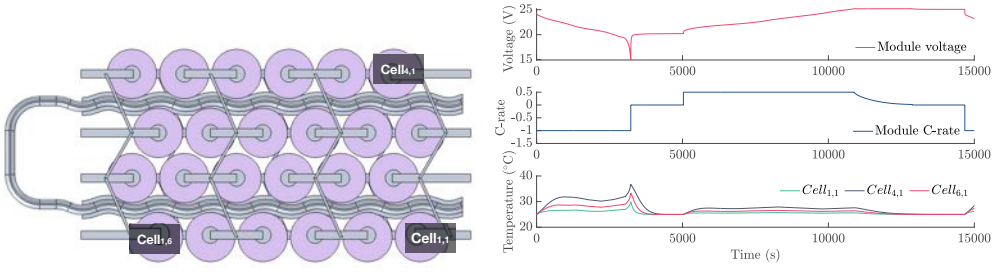

(a) (b)

Fig. 2. (a) The position of the representative cells. (b) One full cycle of voltage, current and temperature change)

The temperature, voltage, and current density at the end of discharge (3200 s) are presented in Fig. 3. Fig. 3a displays the temperature distribution at 3200 s. A maximum temperature difference of approximately 8 °C is observed between parallel-connected cells ($Cell_{1,1}$ and $Cell_{4,1}$), and around 4 °C for serial-connected cells ($Cell_{1,1}$ and $Cell_{1,6}$). These temperature gradients directly affect the current distribution among parallel-connected cells, as cells with shared positive and negative terminals must maintain identical electric potentials, depicted in Fig. 3b. Consequently, the current density among parallel-connected cells varies in response to the temperature gradient, as demonstrated in Fig. 3c.

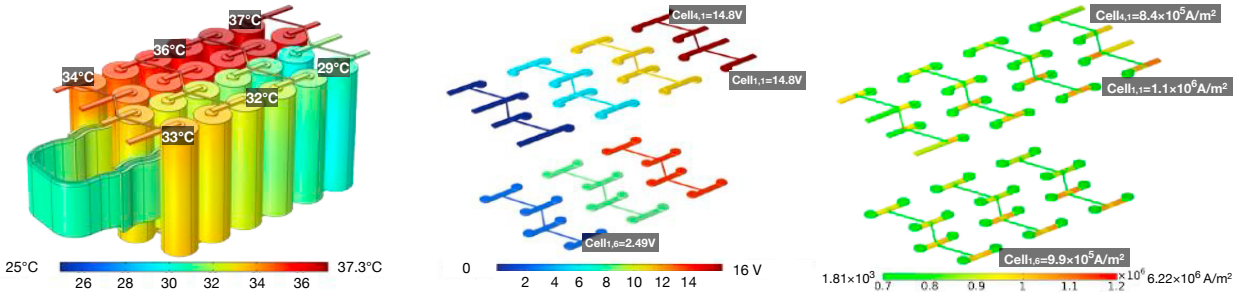

Fig. 3. The distribution of (a) temperature (b) electric potential, and (c) current density at the end of discharging (3200s).

Fig. 4 reveals the imbalanced SOC resulting from the current maldistribution among parallel-connected cells. Fig. 4a illustrates the current change for $Cell_{1,1}$ and $Cell_{4,1}$ over 3200 s. For parallel-connected cells, the current in the higher-temperature $Cell_{4,1}$ increases until approximately 85% depth of discharge (DOD). Beyond this point, $Cell_{4,1}$ approaches full discharge, causing the discharge current to decrease while it increases for the lower-temperature $Cell_{1,1}$. The 8 °C temperature difference results in a current discrepancy of about 0.43 A, leading to an imbalanced discharge process and SOC, as shown in Fig. 4b. It is observed that $Cell_{4,1}$ has the lowest SOC, indicating the highest workload and earliest end-of-life among the cells.

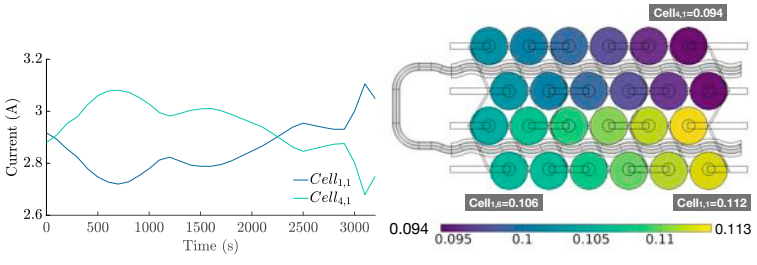

Fig. 4. (a) The current change for $Cell_{1,1}$ and $Cell_{4,1}$. (b) The SOC map at 3200 s.

Fig. 5 illustrates the SOC variation of $Cell_{1,1}$, $Cell_{4,1}$, and $Cell_{1,6}$ over a 30-day period. Among the cells, $Cell_{1,1}$ demonstrates the slowest ageing rate. When comparing the SOH between $Cell_{1,1}$ and the parallel-connected $Cell_{4,1}$, a difference of 0.01 is observed at a maximum temperature difference of 8 °C. On the other hand, the difference between $Cell_{1,1}$ and the serial-connected $Cell_{1,6}$ is 0.003 at a maximum temperature difference of 4 °C. Fig. 5b presents the SOC map of the battery pack at the conclusion of the 30th day. It can observed that the cell ageing rate is primarily influenced by temperature due to 1) cell internal resistance decrease with the increasing temperature and therefore undergoes higher current in the majority of discharging period, which will increase the ageing rate; 2) the high temperature also directly increases the ageing rate. Cells operating at higher temperatures experience premature ageing. This highlights the crucial role of effective BTMS in battery packs to ensure optimal performance and longevity.

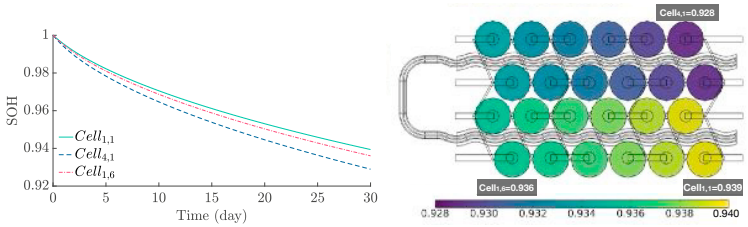

(a) (b)

Fig. 5. (a) SOH change for $Cell_{1,1}$, $Cell_{4,1}$, and $Cell_{1,6}$ and (b) the SOH map after 30 days.

4. Conclusion

This study has investigated the impact of temperature gradients on the uneven ageing of a battery pack, particularly focusing on the performance of parallel-connected and serial-connected cells. The cooling system, cycling protocol, and temperature distribution have been thoroughly analysed, and the influence of temperature gradients on current distribution and SOC has been demonstrated. The results reveal that temperature gradients directly affect the current distribution among parallel-connected cells and lead to imbalanced SOC. It was observed that the cell operating at a higher temperature experienced a higher workload and reached its end of life earlier than other cells. This emphasises the importance of effective BTMS strategies in battery packs to mitigate the impact of temperature gradients, ensuring uniform current distribution, and ultimately prolonging the service life of the entire battery pack.

References

Al-Zareer, M. (2020). Numerical study of flow and heat transfer performance of 3d-printed polymer-based battery thermal management. *International Journal of Heat and Mass Transfer*, 158:119995.

Bernardi, D., Pawlikowski, E., and Newman, J. (1985). A general energy balance for battery systems. *Journal of the electrochemical society*, 132(1):5.

COMSOL (2022). Theory for the lumped battery interface. *The Battery Design Module User's Guide 6.1*, pages 309–315.

Ekström, H. and Lindbergh, G. (2015). A model for predicting capacity fade due to sei formation in a commercial graphite/lifepo4 cell. *Journal of The Electrochemical Society*, 162(6):A1003.

Ekström, H., Fridholm, B., and Lindbergh, G. (2018). Comparison of lumped diffusion models for voltage prediction of a lithium-ion battery cell during dynamic loads. *Journal of Power Sources*, 402:296–300.

Gong, X., Xiong, R., and Mi, C. C. (2014). Study of the characteristics of battery packs in electric vehicles with parallel-connected lithium-ion battery cells. *IEEE Transactions on Industry Applications*, 51(2):1872–1879.

Gümüşsu, E., Ekici, Ö., and Köksal, M. (2017). 3-d cfd modeling and experimental testing of thermal behavior of a li-ion battery. *Applied Thermal Engineering*, 120:484–495.

He, H., Chen, X., Fly, A., and Saini, V. (2023). A fast activation energy derivation (faed) approach for lumped single particle model in lithium-ion battery module-level heat generation prediction. *Journal of Power Sources*, 580:233431.

Jafari, M., Khan, K., and Gauchia, L. (2018). Deterministic models of li-ion battery aging: It is a matter of scale. *Journal of Energy Storage*, 20:67–77.

Lu, Z., Yu, X., Wei, L., Cao, F., Zhang, L., Meng, X., and Jin, L. (2019). A comprehensive experimental study on temperature-dependent performance of lithium-ion battery. *Applied Thermal Engineering*, 158:113800.

Shan, H., Cao, H., Xu, X., Xiao, T., Hou, G., Cao, H., Tang, Y., and Zheng, G. (2022). Investigation of self-discharge properties and a new concept of open-circuit voltage drop rate in lithium-ion batteries. *Journal of Solid State Electrochemistry*, 26(1):163–170.

Tang, Y., Hu, J., Tao, H., Li, Y., Li, W., Li, H., Zhou, M., Wang, K., and Jiang, K. (2022). Rational design of prussian blue analogues as conversion anodes for lithium-ion batteries with high capacity and long cycle life. *Journal of Alloys and Compounds*, 891:161867.

Yang, N., Zhang, X., Shang, B., and Li, G. (2016). Unbalanced discharging and aging due to temperature differences among the cells in a lithium-ion battery pack with parallel combination. *Journal of Power Sources*, 306:733–741.

Zhou, G., Chen, H., and Cui, Y. (2022). Formulating energy density for designing practical lithium–sulfur batteries. *Nature Energy*, 7(4):312–319.

Zhu, W., Lei, F., Zhong, H., and Wang, D. (2023). An improved reliability assessment method for lithium-ion battery system considering imbalanced current and uneven cooling. *Energy*, page 127424.

Ziegler, A., Oeser, D., Hein, T., Montesinos-Miracle, D., and Ackva, A. (2021). Reducing cell to cell variation of lithium-ion battery packs during operation. *IEEE access*, 9:24994–25001.